

可调谐四宽带太赫兹吸收器设计

张婷^{1,2*}, 郭泰铭³, 闫俊伢¹, 裴娅男¹¹山西工程科技职业大学信息工程学院, 山西 晋中 030619;²中北大学仪器与电子学院, 山西 太原 030051;³昆士兰大学, 澳大利亚 昆士兰 布里斯班 4072

摘要 设计了一种四宽带且吸收率动态可调的太赫兹吸收器,该吸收器结构简单,由顶层二氧化钒、中间层二氧化硅和底层金属组成。仿真结果表明,在0~10 THz范围内,吸收率超过90%的吸收带共有4个,带宽分别为0.87、0.58、0.61、0.45 THz。随二氧化钒电导率的变化,吸收率可在7.7%~99.9%范围内动态调节。引入阻抗匹配理论和法布里-珀罗共振理论解释了吸收器的物理机理,并通过电场分布分析了多个完美吸收峰的物理来源。此外,该吸收器还具有偏振不敏感和广角吸收的特点,可在微辐射计、生物传感器和隐身技术等应用领域应用。

关键词 光学器件; 超材料; 太赫兹吸收器; 可调谐吸收器; 宽带

中图分类号 O441

文献标志码 A

DOI: 10.3788/AOS231751

1 引言

电磁超材料是利用现有材料人工设计成的单元结构,具有一些超越自然性质的特性。自从负折射率材料^[1]、金属线组成的超材料^[2-4]被提出后,超材料受到科学界的广泛关注。超材料在很多领域得到发展应用,比如完美吸收器^[5-7]、光学透镜^[8-9]和隐形斗篷^[10-11]等。其中,自从第一个超材料完美吸收器(MPA)被Landy等^[12]提出后,MPA在微波辐射计^[13-15]、生物传感器^[16-17]、热辐射器^[18-19]和成像^[20]等领域的应用范围迅速扩大。

这些MPA大部分是单频点或者多频点的,例如张晓健等^[21]设计的两频点吸收器、张向等^[22]设计的具有4个频点的吸收器,这些吸收器都存在频带窄的问题,不能满足某些光电器件的需求。为了解决此问题,通常采用在同一层单元中构造不同图形,或者不同图形多层叠加的结构。然而,这些结构往往比较复杂,且存在吸收率不能主动调节的问题。近年来,超材料设计中引用了各种可变材料^[23-28],从而使这些器件的光学性能能够被主动控制。二氧化钒(VO_2)就是一种可控的功能材料,它可以被热、电或光^[29]激发,实现从绝缘状态到金属状态的变换。近期,很多学者报道了使用 VO_2 设计的宽带MPA,例如:Song等^[30]提出一种吸收率变化范围为30%~100%的宽带吸收器,其中吸

收率大于90%的带宽为0.33 THz;Hu等^[31]提出一种双宽带吸收器,95%以上吸收率的带宽为0.5 THz和0.6 THz。Huang等^[32]设计了一种80%以上吸收率的带宽分别为0.88 THz和0.77 THz的双宽带吸收器。但是,这些MPA均存在频带较窄或频带数量较少的问题。

根据多个尺寸吸收器叠加的逻辑,可以获得很多吸收带,但实际上,由4个不同大小的谐振器组成的超级谐振器^[33],相邻谐振器的相互作用非常大,要想利用不同尺寸的谐振器实现4个频带以上的超级谐振器是非常困难的。令人欣慰的是,最近一些小组的研究同时激发了基模和高阶模态共振,如环形矩形腔^[34]、多层光栅^[35]等,但是利用高阶模态所激发的吸收率一般小于50%。可见,综合优化多频带、宽带和可调谐这3个特性仍是一项很有意义的工作。

本文提出一种在0~10 THz内具有4个宽带的太赫兹吸收器,其结构较为简单。随着温度或者光照变化,所提吸收器的吸收率在7.7%~99.9%内动态可调。讨论了吸收器的顶层和中间介质层变化对吸收器性能的影响,分析了4个吸收峰的机理和来源,并分析了极化角和入射角对吸收性能的影响。本研究可以在一定程度上促进生物传感器、光电器件等太赫兹器件的应用。

收稿日期: 2023-11-07; 修回日期: 2023-11-30; 录用日期: 2023-12-13; 网络首发日期: 2023-12-23

基金项目: 国家自然科学基金(61501213)、山西省基础研究计划(自由探索类)青年科学研究项目(202203021222127)、山西工程科技职业大学校科研基金(KJ202221)

通信作者: *zhangting_cai@163.com

2 结构模型和方法

所设计的超材料吸收器为三层结构,上层是 VO₂ 层,中间层是二氧化硅(SiO₂)层,下层是金(Au)接地层,图 1(a)为吸收器的阵列结构示意图。底层 Au 的电导率 $\sigma_{Au}=4.56 \times 10^7$ S/m,厚度为 0.2 μm 。中间层 SiO₂ 的相对介电常数 $\epsilon_{SiO_2}=3.9+0.03i$,厚度为 30 μm 。VO₂ 层的厚度为 0.2 μm 。吸收器结构单元的顶视图如图 1(b)所示,单元阵列为正方形,边长为 p 。VO₂ 图形为十字形加矩形四臂,矩形四臂对称分布在十字四周。十字形长为 l_1 ,四臂长为 l_2 ,宽 $w_1=w_2$,四臂距中心的距离为 X 。经过优化,图 1 中 $p=75 \mu\text{m}$ 、 $l_1=68 \mu\text{m}$ 、 $l_2=19 \mu\text{m}$ 、 $w_1=w_2=9 \mu\text{m}$ 、 $X=21 \mu\text{m}$ 。

为了有效研究吸收器的性能,采用基于有限积分技术的微波仿真软件 CST Microwave Studio 2020 对所提结构进行仿真。VO₂ 的光学性能可以由 Drude 模型^[36-37]描述,即

$$\epsilon(\omega) = \epsilon_{\infty} - \frac{\omega_p^2(\sigma)}{\omega^2 + i\gamma\omega}, \quad (1)$$

式中: $\epsilon_{\infty}=12$ 为无穷处频率; $\gamma=5.75 \times 10^{13}$ rad/s 为碰撞频率; $\omega_p(\sigma)$ 为电导依赖等离子体频率,可近似写作 $\omega_p^2(\sigma) = \frac{\sigma}{\sigma_0} \omega_p^2(\sigma_0)$,其中 $\sigma_0 = 3 \times 10^5$ S/m, $\omega_p(\sigma_0) = 1.4 \times 10^{15}$ rad/s; ω 为角频率。

之前的研究表明,当温度从 298 K(室温)增加到 340 K 时,VO₂ 会从绝缘态转变为金属态,其电导率可以从 200 S/m 调整到 2×10^5 S/m^[38-39]。

吸收器的吸收率 $A(\omega)$ 可通过仿真提取的反射系数 $S_{11}(\omega)$ 和透射系数 $S_{21}(\omega)$ 求得,即 $A(\omega) = 1 - R(\omega) - T(\omega) = 1 - |S_{11}(\omega)|^2 - |S_{21}(\omega)|^2$,其中, $R(\omega)$ 为反射率, $T(\omega)$ 为透射率。入射波在金属薄膜中的趋肤深度远远小于底层金属的厚度,使得透射率 $T(\omega)$ 接近 0。因此,吸收率可以简化为 $A(\omega) = 1 - R(\omega) = 1 - |S_{11}(\omega)|^2$,可见,当反射率也为 0 时,可以实现完美吸收。

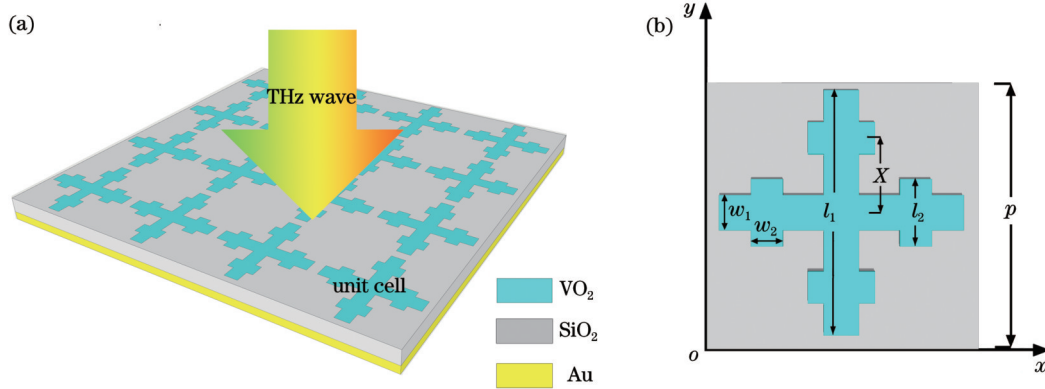


图 1 宽带吸收器结构图。(a)整个阵列图;(b)单个单元顶视图

Fig. 1 Diagram of broadband absorber structure. (a) Schematic of complete array; (b) top view of unit

3 分析与讨论

3.1 结果分析

如图 2(a)所示,当 THz 波垂直入射时,该吸收器 90% 以上吸收率的带宽分别为 0.87、0.58、0.61、0.45 THz,分布在 0.76~1.63 THz、3.46~4.04 THz、6.11~6.72 THz、8.68~9.13 THz 范围内,相应的相对带宽分别为 73%、15%、10% 和 5%。可见,在 0~10 THz 范围内共有 4 个吸收宽带^[40]。通过温度来控制 VO₂ 的电导率变化,当电导率从 200 S/m 变化到 2×10^5 S/m 时,相应的第一宽带吸收率可从 7.7% 动态调整到 99.7%,第二宽带吸收率可从 16.6% 动态调整到 99.9%,第三宽带吸收率可从 24.4% 动态调整到 99.5%,第四宽带吸收率可从 34.3% 动态调整到 99.1%,并且各个吸收带中吸收峰的中心位置基本保持不变。出现这个结果的原因是 VO₂ 介电常数的变

化。图 2(b)、(c)所示分别为不同电导率下,VO₂ 介电常数实部和虚部的变化曲线。可以看出,VO₂ 介电常数的实部变化比虚部变化要小得多,这就导致了 VO₂ 介电常数变化时,谐振频率几乎不变而吸收率变化较大。

3.2 介质层和顶层分析

研究了介质层 SiO₂ 和顶层 VO₂ 对吸收性能的影响。图 3 所示为 TE 极化时,去掉顶层 VO₂、VO₂ 为四臂形、VO₂ 为十字形以及完整吸收结构的吸收情况。由去掉顶层 VO₂ 的吸收曲线(点划线)可知,吸收率低于 32%。在 1.40、3.84、6.35、8.88 THz 处出现 4 个吸收峰,它们的频率间隔均值为 2.49 THz。由于介质层产生法布里-珀罗共振^[41],相邻吸收峰值之间的频率间隔可以写为 $\Delta f = \frac{c_0}{2nd \cos \theta}$,其中 c_0 为真空中的光速, θ 为 THz 波的入射角度, d 为介质层的厚度, n 为介

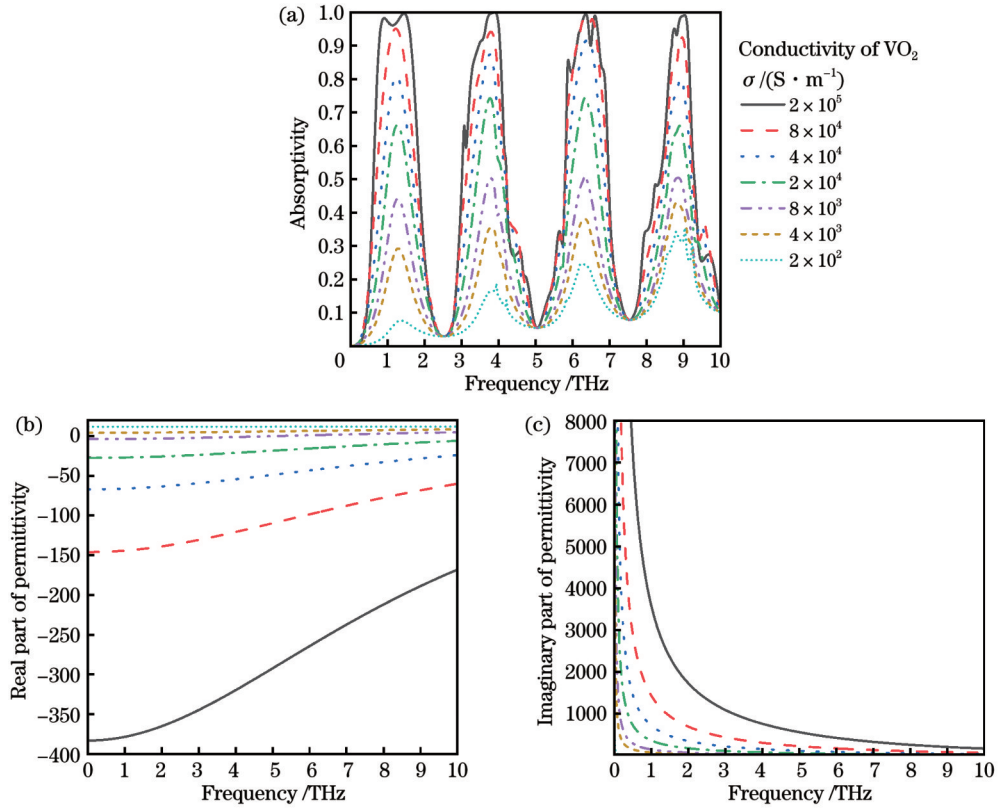


图 2 吸收率、介电常数实部和虚部随 VO₂电导率的变化。(a)吸收率随 VO₂电导率的变化;(b)介电常数实部随 VO₂电导率的变化;(c)介电常数虚部随 VO₂电导率的变化

Fig. 2 Absorption and real part and imaginary part of the permittivity with different conductivities of VO₂. (a) Absorption with different conductivities of VO₂; (b) real part of permittivity with different conductivities of VO₂; (c) imaginary part of permittivity with different conductivities of VO₂

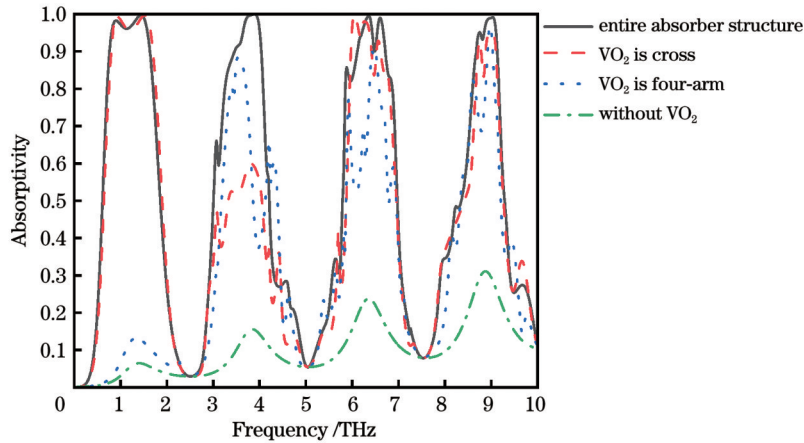


图 3 去掉 VO₂、VO₂为四臂形、VO₂为十字形以及完整吸收结构的吸收曲线

Fig. 3 Absorption curves of without VO₂, VO₂ is cross, VO₂ is four-arm, and entire absorber structure

质层的折射率,且 $n = \sqrt{\epsilon_{\text{SiO}_2}}$ 。理论计算出频率间隔为 2.53 THz,和去掉顶层 VO₂时的仿真结果几乎一致。由图 3 所示的完整吸收结构的吸收曲线(实线)可知,在 1.44、3.89、6.63、9.03 THz 处出现 4 个吸收峰,频率间隔均值为 2.53 THz,和未添加顶层时的理论值接近。

在顶层设计了 VO₂ 图形结构。如图 3 所示,十字形 VO₂(短划线)和四臂形 VO₂(点线)单独作用时的吸

收峰位置接近,但是吸收率均较低。当二者组合时,吸收率增大并且得到了宽带吸收。可见,增加了 VO₂ 后,在 VO₂ 金属态时得到更大的带宽和更高的吸收率。

图 4(a)展示了 SiO₂ 的厚度 t_1 分别为 28 μm、30 μm 和 32 μm 时的吸收谱线。随着 SiO₂ 厚度的增加,吸收峰的位置发生了红移,可见 SiO₂ 厚度主要影响吸收峰的位置,对吸收率的影响不大。当厚度为 30 μm 时,吸

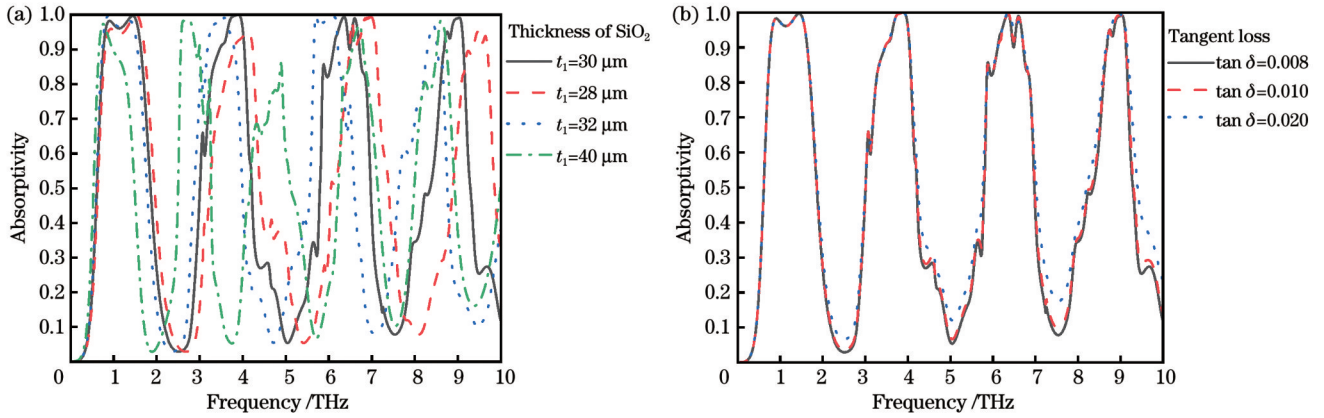


图 4 吸收光谱随 SiO₂ 厚度及损耗正切值的变化。(a) 吸收光谱随 SiO₂ 厚度变化；(b) 吸收光谱随 SiO₂ 损耗正切值变化

Fig. 4 Absorption spectra under different thicknesses and tangent losses of SiO₂. (a) Absorption spectra under different thicknesses of SiO₂; (b) absorption spectra under different tangent losses of SiO₂

收效果最好。当 SiO₂ 厚度继续增大到 40 μm 时, 如图 4(a) 点划线所示, 此时吸收带增加到 5 个, 如果对顶层 VO₂ 进行设计来进一步实现阻抗匹配, 可为更多频带吸收器设计提供思路。图 4(b) 所示为 SiO₂ 在不同损耗正切值 $\tan \delta$ 下的吸收谱线。研究发现, 当 $\tan \delta$ 发生变化时, 其吸收几乎是恒定的, 这说明吸收的主要影响因素不是介质层的损耗, 而是结构设计。

3.3 完美吸收机理

该设计的完美吸收基于阻抗匹配理论^[42-43]。吸收率和相对阻抗之间的关系为

$$A(\omega) = 1 - R(\omega) = 1 - \left| \frac{Z - Z_0}{Z + Z_0} \right|^2 = 1 - \left| \frac{Z_r - 1}{Z_r + 1} \right|^2, \quad (2)$$

$$Z_r = \sqrt{\frac{[1 + S_{11}(\omega)]^2 - S_{21}(\omega)^2}{[1 - S_{11}(\omega)]^2 - S_{21}(\omega)^2}}, \quad (3)$$

式中: Z 为吸收器的阻抗; Z_0 为自由空间的阻抗; $S_{11}(\omega)$ 和 $S_{21}(\omega)$ 分别为反射和透射的 S 参数; $Z_r = Z/Z_0$ 为吸收器相对阻抗。

由式(2)可知, 当相对阻抗等于 1 时, 吸收率最大。如图 5 所示, 随着电导率的增加, 在 4 个频带内 VO₂ 相对阻抗的实部逐渐接近 1, 虚部慢慢变为 0, 此时相对阻抗为 1, 说明吸收器与自由空间的阻抗慢慢匹配。当 VO₂ 的电导率为 2×10^5 S/m 时, 合适的介质层厚度和顶层 VO₂ 图形让吸收器和自由空间的阻抗匹配, 使得所设计吸收器达到最高吸收率和最大工作带宽。

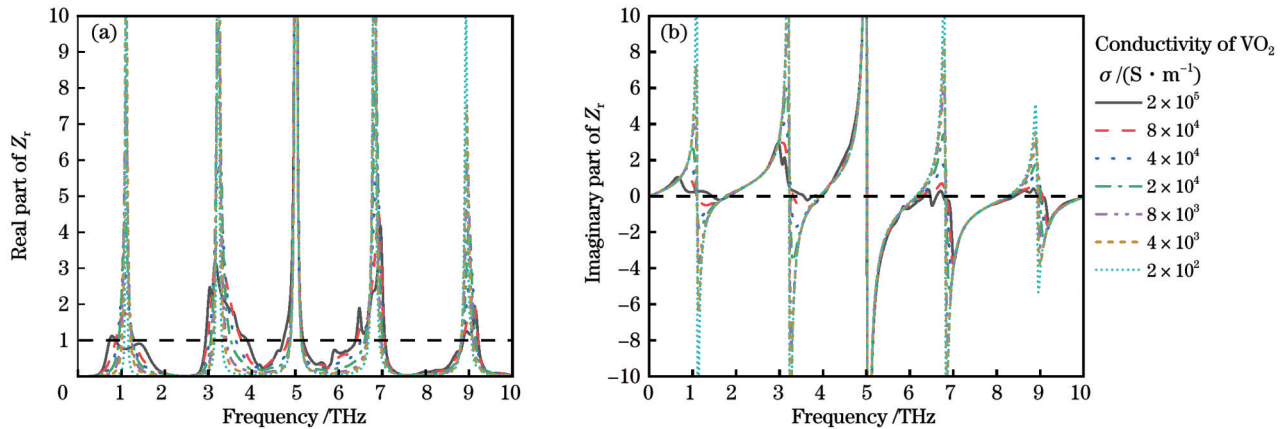


图 5 吸收器相对阻抗随电导率的变化。(a) 相对阻抗的实部; (b) 相对阻抗的虚部

Fig. 5 Relative impedance at different VO₂ conductivities. (a) Real part of relative impedance; (b) imaginary part of relative impedance

为了进一步了解宽带吸收的物理来源, 图 6 给出了 xoy 平面上 4 个近乎完美吸收峰的电场分布, 图中正电场用“+”标出, 负电场用“-”标出。由图 6(a) 可知, 在 $f_1 = 1.44$ THz 处, 在十字纵臂两端有两个大小相等但符号相反的极点, 说明电偶极子共振被激发, 且为

基模。由图 6(b) 可知, 在 $f_2 = 3.89$ THz 处, 两个大小相等但是符号相反的电荷在十字纵臂两端和横臂两端聚集, 说明电偶极子被激发, 且此处的电偶极子对数比 f_1 处增加, 说明此处激发了电偶极子共振的高阶模态^[44]。由图 6(c) 可知, 在 $f_3 = 6.63$ THz 处, 在十字的横臂和上

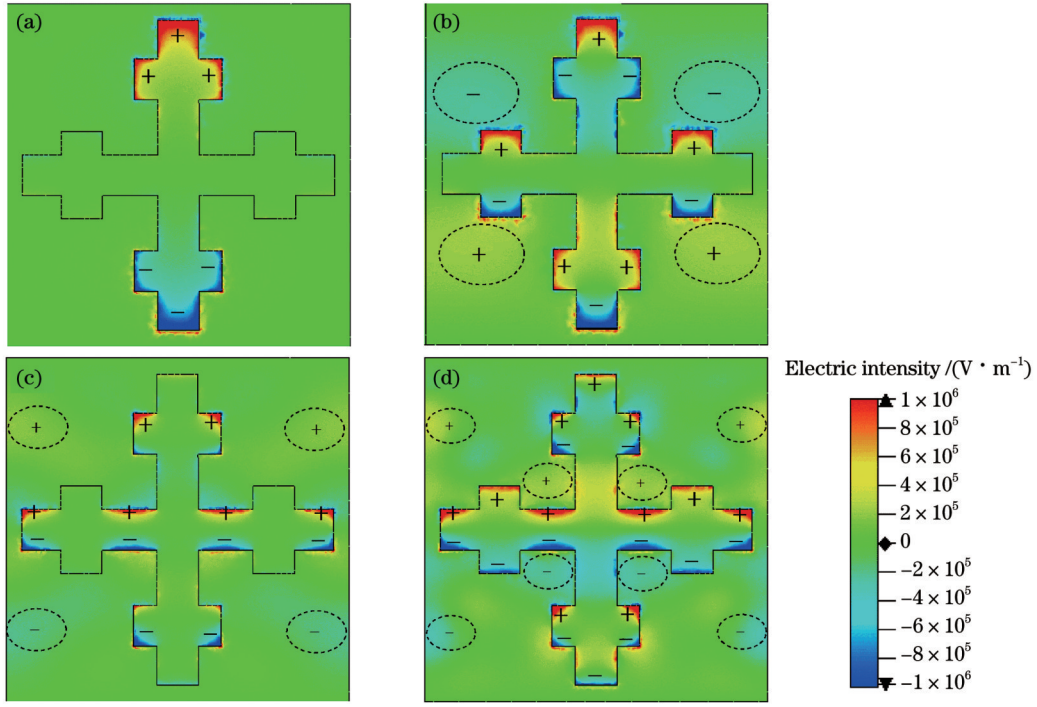


图 6 4 个吸收峰的表面电场分布。(a) $f_1=1.44$ THz; (b) $f_2=3.89$ THz; (c) $f_3=6.63$ THz; (d) $f_4=9.03$ THz

Fig. 6 Surface electric field distribution at four absorption peaks. (a) $f_1=1.44$ THz; (b) $f_2=3.89$ THz; (c) $f_3=6.63$ THz; (d) $f_4=9.03$ THz

下两个横臂处均有大小相等但符号相反的电荷聚集,说明此处激发了电偶极子共振的高阶模式。由图 6(d)可知,在 $f_4=9.03$ THz 处,十字的横纵臂和四臂上均有大小相等但符号相反的电荷集聚,说明此处有更多的电偶极子共振被激发。另外,从图 3 和图 4 都可以看到,第一宽带吸收峰较为光滑,第二~四宽带吸收峰不是很光滑,出现这种现象的原因是,第一宽带的成因主要是 VO_2 的局部吸收,第二~四宽带的成因除了 VO_2 不同部位的局部吸收外,还有介质层与 VO_2 和金属层的耦合作用(图 6 椭圆虚线圈出位置)^[45]。可见,所设计的吸收器不仅能激发基模,还能激发高阶模式,最后构成了多宽带吸收。

3.4 广角吸收及偏振不敏感

不同极化角和入射角下吸收器吸收率的变化如图 7 所示。对于 TE 模式入射,如图 7(a)所示,第一宽带和第二宽带在入射角增大到 60° 之前保持良好的性能,当入射角继续增大时,第一宽带和第二宽带的吸收率出现下降。对于第三、第四宽带,入射角在 30° 内变化时,对吸收率和带宽的影响较小,当入射角度继续增大时,它们的中心频率出现蓝移,带宽逐渐缩小。对于 TM 模式,如图 7(b)所示,当入射角从 0° 增大到 60° 时,吸收率大于 80% ,随着入射角的增大,第三和第四宽带出现蓝移。图 7(c)所示为不同极化角下的吸收光谱。很明显,所设计的吸收器具有很好的极化不敏感特性,这是因为该结构具有旋转对称性^[46]。

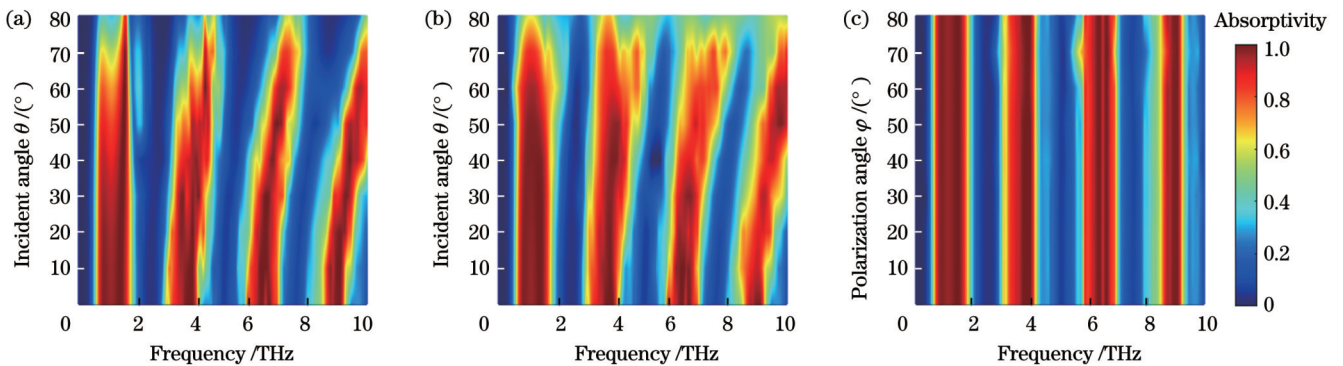


图 7 入射角和偏振角对吸收的影响。(a) TE 模式入射角的影响; (b) TM 模式入射角的影响; (c) TE 模式极化角的影响

Fig. 7 Effect of incidence and polarization angles on absorption. (a) Effect of incidence angle in TE mode; (b) effect of incidence angle in TM mode; (c) effect of polarization angle in TE mode

4 结 论

提出一种多宽带、吸收主动可调的宽带吸收器, 其由 MPA 的三层结构组成。结果表明, 吸收率超过 90% 的宽带共有 4 个, 带宽分别为 0.87、0.58、0.61、0.45 THz。通过使用热控制来诱导 VO₂ 电导率变化, 吸收器的吸收率可从 7.7% 动态调整到 99.9%。为了解释所设计吸收器的物理机理, 引入了法布里-珀罗共振和阻抗匹配理论。通过对电场分布的分析发现, 第一个宽带主要是由 VO₂ 的局部吸收引起的, 第二~四宽带的形成除了有 VO₂ 表面多个电偶极子共振吸收外, 还有介质层与 VO₂ 和金属层之间的耦合效应所引起的吸收。此外, 所设计的吸收器具有极化不敏感特性和良好的广角吸收性能, 在成像、调制、传感和隐身方面有很大的应用潜力。

参 考 文 献

- [1] Shelby R A, Smith D R, Schultz S. Experimental verification of a negative index of refraction[J]. *Science*, 2001, 292(5514): 77-79.
- [2] Yuan Y, Bingham C, Tyler T, et al. A dual-resonant terahertz metamaterial based on single-particle electric-field-coupled resonators[J]. *Applied Physics Letters*, 2008, 93(19): 191110.
- [3] Ogando K, Pastoriza H. Design of integration-ready metasurface-based infrared absorbers[J]. *Journal of Applied Physics*, 2015, 118(4): 043109.
- [4] Wu K M, Huang Y J, Wang H T L, et al. Numerical and theoretical analysis on the absorption properties of metasurface-based terahertz absorbers with different thicknesses[J]. *Applied Optics*, 2015, 54(2): 299-305.
- [5] Bao Z Y, Wang J C, Hu Z D, et al. Coordinated multi-band angle insensitive selection absorber based on graphene metamaterials[J]. *Optics Express*, 2019, 27(22): 31435-31445.
- [6] Bao Z Y, Wang J C, Hu Z D, et al. Coordination multi-band absorbers with patterned irrelevant graphene patches based on multi-layer film structures[J]. *Journal of Physics D*, 2021, 54(50): 505306.
- [7] Song N T, Sun Q, Xu S, et al. Ultrawide-band optically transparent antidiffraction metamaterial absorber with a Thiessen-polygon metal-mesh shielding layer[J]. *Photonics Research*, 2023, 11(7): 1354-1363.
- [8] Pendry J B. Negative refraction makes a perfect lens[J]. *Physical Review Letters*, 2000, 85(18): 3966-3969.
- [9] 唐剑雄, 龚岩栋, 庞恺. 二维超构表面: 超透镜应用及研究进展[J]. *激光与光电子学进展*, 2023, 60(21): 2100004. Tang J X, Gong Y D, Pang K. Two-dimensional metasurface: application and research progress of metalenses[J]. *Laser & Optoelectronics Progress*, 2023, 60(21): 2100004.
- [10] Bilotti F, Tricarico S, Vegni L. Plasmonic metamaterial cloaking at optical frequencies[J]. *IEEE Transactions on Nanotechnology*, 2010, 9(1): 55-61.
- [11] Schurig D, Mock J J, Justice B J, et al. Metamaterial electromagnetic cloak at microwave frequencies[J]. *Science*, 2006, 314(5801): 977-980.
- [12] Landy N I, Sajuyigbe S, Mock J J, et al. Perfect metamaterial absorber[J]. *Physical Review Letters*, 2008, 100(20): 207402.
- [13] Zong S, Zeng D W, Yuan W, et al. Recent advances on perfect light absorbers and their promise for high-performance optoelectronic devices[J]. *Chinese Optics Letters*, 2022, 20(7): 073603.
- [14] Maier T, Brueckl H. Multispectral microbolometers for the midinfrared[J]. *Optics Letters*, 2010, 35(22): 3766-3768.
- [15] Grant J, Escorcia-Carranza I, Li C, et al. A monolithic resonant terahertz sensor element comprising a metamaterial absorber and micro-bolometer[J]. *Laser & Photonics Reviews*, 2013, 7(6): 1043-1048.
- [16] Jing X F, Qin G H, Zhang P. Broadband silicon-based tunable metamaterial microfluidic sensor[J]. *Photonics Research*, 2022, 10(12): 2876-2885.
- [17] Li R F, Wu D, Liu Y M, et al. Infrared plasmonic refractive index sensor with ultra-high figure of merit based on the optimized all-metal grating[J]. *Nanoscale Research Letters*, 2017, 12(1): 1.
- [18] Karalis A, Joannopoulos J D. 'Squeezing' near-field thermal emission for ultra-efficient high-power thermophotovoltaic conversion[J]. *Scientific Reports*, 2016, 6: 28472.
- [19] Xiao D, Tao K Y. Ultra-compact metamaterial absorber for multiband light absorption at mid-infrared frequencies[J]. *Applied Physics Express*, 2015, 8(10): 102001.
- [20] Ouchi T, Kajiki K, Koizumi T, et al. Terahertz imaging system for medical applications and related high efficiency terahertz devices[J]. *Journal of Infrared, Millimeter, and Terahertz Waves*, 2014, 35(1): 118-130.
- [21] 张晓健, 张权, 兰桂莲, 等. 基于塔姆等离激元的硼烯近完美吸收器[J]. *光子学报*, 2023, 52(10): 1052404. Zhang X J, Zhang Q, Lan G L, et al. Nearly perfect absorber in borophene based on Tamm plasmon polaritons[J]. *Acta Photonica Sinica*, 2023, 52(10): 1052404.
- [22] 张向, 王玥, 张婉莹, 等. 单壁碳纳米管太赫兹超表面窄带吸收及其传感特性研究[J]. *物理学报*, 2024, 73(2): 026102. Zhang X, Wang Y, Zhang W Y, et al. Narrow band absorption and sensing properties of the THz metasurface based on single-walled carbon nanotubes[J]. *Acta Physica Sinica*, 2024, 73(2): 026102.
- [23] Shin J H, Park K H, Ryu H C. Electrically controllable terahertz square-loop metamaterial based on VO₂ thin film[J]. *Nanotechnology*, 2016, 27(19): 195202.
- [24] Xu Z H, Wu D, Liu Y M, et al. Design of a tunable ultra-broadband terahertz absorber based on multiple layers of graphene ribbons[J]. *Nanoscale Research Letters*, 2018, 13(1): 143.
- [25] Zhai Z C, Zhang L, Li X J, et al. Tunable terahertz broadband absorber based on a composite structure of graphene multilayer and silicon strip array[J]. *Optics Communications*, 2019, 431: 199-202.
- [26] 朱华利, 张勇, 叶龙芳, 等. 基于石墨烯-二氧化钒的太赫兹双控可调宽带吸收器[J]. *光学学报*, 2022, 42(14): 1423002. Zhu H L, Zhang Y, Ye L F, et al. Dual-control and tunable broadband terahertz absorber based on graphene-vanadium dioxide[J]. *Acta Optica Sinica*, 2022, 42(14): 1423002.
- [27] Song Z Y, Wang Z S, Wei M L. Broadband tunable absorber for terahertz waves based on isotropic silicon metasurfaces[J]. *Materials Letters*, 2019, 234: 138-141.
- [28] 陈宇婷, 薛文瑞, 张敬, 等. 基于二氧化钒的动态可调谐的红外线超宽带吸收器[J]. *中国激光*, 2023, 50(19): 1913001. Chen Y T, Xue W R, Zhang J, et al. Dynamically tunable infrared ultra-wideband absorber based on vanadium dioxide[J]. *Chinese Journal of Lasers*, 2023, 50(19): 1913001.
- [29] Jepsen P U, Fischer B M, Thoman A, et al. Metal-insulator phase transition in a VO₂ thin film observed with terahertz spectroscopy[J]. *Physical Review B*, 2006, 74(20): 205103.
- [30] Song Z Y, Wang K, Li J W, et al. Broadband tunable terahertz absorber based on vanadium dioxide metamaterials[J]. *Optics Express*, 2018, 26(6): 7148-7154.
- [31] Hu N, Wu F L, Bian L A, et al. Dual broadband absorber based on graphene metamaterial in the terahertz range[J]. *Optical Materials Express*, 2018, 8(12): 3899-3909.

- [32] Huang J, Li J N, Yang Y, et al. Active controllable dual broadband terahertz absorber based on hybrid metamaterials with vanadium dioxide[J]. *Optics Express*, 2020, 28(5): 7018-7027.
- [33] Wang B X, Zhai X, Wang G Z, et al. Design of a four-band and polarization-insensitive terahertz metamaterial absorber[J]. *IEEE Photonics Journal*, 2015, 7(1): 4600108.
- [34] Dayal G, Solanki A, Chin X Y, et al. High-Q plasmonic infrared absorber for sensing of molecular resonances in hybrid lead halide perovskites[J]. *Journal of Applied Physics*, 2017, 122(7): 073101.
- [35] Liu X Y, Gao J S, Yang H G, et al. Multiple infrared bands absorber based on multilayer gratings[J]. *Optics Communications*, 2018, 410: 438-442.
- [36] Bai J J, Zhang S S, Fan F, et al. Tunable broadband THz absorber using vanadium dioxide metamaterials[J]. *Optics Communications*, 2019, 452: 292-295.
- [37] Wang T L, Zhang Y P, Zhang H Y, et al. Dual-controlled switchable broadband terahertz absorber based on a graphene-vanadium dioxide metamaterial[J]. *Optical Materials Express*, 2020, 10(2): 369-386.
- [38] Lian Y, Li Y K, Lou Y P, et al. Adjustable trifunctional mid-infrared metamaterial absorber based on phase transition material VO₂[J]. *Nanomaterials*, 2023, 13(12): 1829.
- [39] 王岩, 陈哲, 崔琦. 基于二氧化钒的可调谐太赫兹宽带带通滤波器[J]. *光学学报*, 2021, 41(20): 2023002.
Wang Y, Chen Z, Cui Q. A tunable terahertz broadband bandpass filter based on vanadium dioxide[J]. *Acta Optica Sinica*, 2021, 41(20): 2023002.
- [40] Song Z Y, Wei M L, Wang Z S, et al. Terahertz absorber with reconfigurable bandwidth based on isotropic vanadium dioxide metasurfaces[J]. *IEEE Photonics Journal*, 2019, 11(2): 4600607.
- [41] Zhao Z Y, Zhao H W, Peng W, et al. Polarization dependence of terahertz Fabry-Pérot resonance in flexible complementary metamaterials[J]. *Plasmonics*, 2015, 10(6): 1587-1592.
- [42] Zhao Y, Huang Q P, Cai H L, et al. A broadband and switchable VO₂-based perfect absorber at the THz frequency[J]. *Optics Communications*, 2018, 426: 443-449.
- [43] 樊浩田, 薛文瑞, 陈宇婷, 等. 基于金属铼和二氧化硅材料的紫外线超宽带吸收器[J]. *中国激光*, 2024, 51(2): 0213003.
Fan H T, Xue W R, Chen Y T, et al. Ultra-wideband UV absorber based on rhodium metal and silica materials[J]. *Chinese Journal of Lasers*, 2024, 51(2): 0213003.
- [44] Zhao L, Liu H, He Z H, et al. Theoretical design of twelve-band infrared metamaterial perfect absorber by combining the dipole, quadrupole, and octopole plasmon resonance modes of four different ring-strip resonators[J]. *Optics Express*, 2018, 26(10): 12838-12851.
- [45] Wang J C, Wang X Y, Hu Z D, et al. Independent tunable multi-band absorbers based on molybdenum disulfide metasurfaces[J]. *Physical Chemistry Chemical Physics*, 2019, 21(43): 24132-24138.
- [46] Zhu B, Wang Z B, Huang C, et al. Polarization insensitive metamaterial absorber with wide incident angle[J]. *Progress in Electromagnetics Research*, 2010, 101: 231-239.

Design of Tunable Four-Broadband Terahertz Absorber

Zhang Ting^{1,2*}, Guo Taiming³, Yan Junya¹, Pei Yanan¹

¹College of Information Engineering, Shanxi Vocational University of Engineering Science and Technology, Jinzhong 030619, Shanxi, China;

²College of Instrumentation and Electronics, North University of China, Taiyuan 030051, Shanxi, China;

³The University of Queensland, Brisbane 4072, Queensland, Australia

Abstract

Objective Since the first metamaterial perfect absorber was proposed by Landy *et al.*, it has been widely developed due to its potential applications in the fields of microwave radiation measurement, biosensors, thermal emitters, and imaging. Many existing absorbers face the issue of narrow bandwidths, which fail to satisfy the demands of some optoelectronic devices. To solve this problem, it is common to construct different patterns in the same layer or stack multilayer structures with different geometrical dimensions. However, these structures are often complex, and the absorption rate cannot be actively adjusted. Therefore, phase change materials have been introduced to regulate the absorption rate of absorbers, and vanadium dioxide is one of them. There are many absorbers designed with VO₂, but the absorption bandwidth and band number need to be further increased. Therefore, combining the characteristics of multi-band, wideband, and tunable absorption remains a meaningful endeavor.

Methods To effectively study the performance of the absorber, the proposed structure is analyzed by using the microwave simulation software CST Microwave Studio 2020. The metamaterial absorber in this study consists of three layers: the top layer VO₂, the middle layer SiO₂, and the bottom layer Au. When the conductivity is adjusted from 200 S/m to 2 × 10⁵ S/m, VO₂ will change from an insulator to metal, which can be simulated by input conductivity parameters through the Drude model in CST software. The absorber's absorption can be obtained through one minus the reflection and transmission. Since the penetration depth of the incident wave is smaller than the Au thickness, thus the transmittance is zero. Perfect absorption can be achieved when the reflection is also zero. Material selection and structural design are used to

achieve impedance matching, ensuring zero reflection and ultimately realizing perfect absorption of multiple broadbands.

Results and Discussions The simulation results show that there are four absorption bands with more than 90% of absorptivity in the range of 0–10 THz, covering bandwidths of 0.87, 0.58, 0.61, and 0.45 THz, respectively. With variations in the conductivity of VO₂, the absorptivity dynamically adjusts between 7.7% and 99.9% (Fig. 2). The analysis finds that with the change of dielectric constant of vanadium dioxide, the resonant frequency remains almost constant, while the absorption rate changes significantly. The Fabry-Perot resonance theory and impedance matching theory are introduced to explain the effects of the dielectric layer and the VO₂ layer on the absorption (Figs. 3–5). The physical sources of multiple perfect absorption peaks are analyzed through the electric field distribution (Fig. 6). Additionally, changes in absorptivity with different incident angles and polarization angles are analyzed (Fig. 7), which shows that the absorber has the characteristics of polarization insensitivity and wide-angle absorption.

Conclusions We describe a terahertz absorber with four absorption bands, dynamically adjustable absorptivity, and a simple structure. Simulation results indicate that within the range of 0–10 THz, there are four absorption bands with more than 90% absorptivity, and their respective bandwidths are 0.87, 0.58, 0.61, and 0.45 THz. The absorptivity can be dynamically adjusted between 7.7% and 99.9% by varying the conductivity of vanadium dioxide. The physical mechanism of the absorber is explained using impedance matching theory and Fabry-Perot resonance theory. Through the analysis of the electric field distribution, it is found that the first broadband absorption is mainly caused by the local absorption of VO₂, while the second, third, and fourth broadband absorptions result from the resonance absorption of multiple electric dipoles on the surface of VO₂, coupled with the coupling effects between the dielectric layer and VO₂ and the metal layer. Additionally, it has the features of wide-angle absorption and polarization insensitivity. This absorber has potential applications in micro-radiometers, biosensors, stealth technology, and other fields.

Key words optical device; metamaterials; terahertz absorber; tunable absorber; broadband